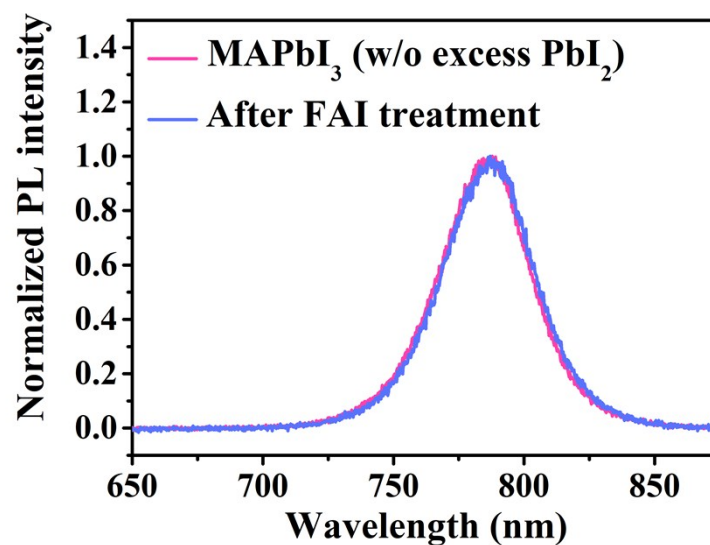


## Electronic Supplementary Information

### Synchronous Surface and Bulk Composition Management for Red-shifted Light Absorption and Suppressed Interfacial Recombination in Perovskite Solar Cells

*Jun-Xing Zhong<sup>a</sup>, Jin-Feng Liao<sup>a</sup>, Yong Jiang<sup>a</sup>, Lianzhou Wang<sup>\*b</sup>, Dai-Bin Kuang<sup>\*a</sup> and Wu-Qiang Wu<sup>\*ab</sup>*



**Fig. S1** PL spectra of MAPbI<sub>3</sub> (without 1 mol% excess PbI<sub>2</sub>) before and after FAI treatment.

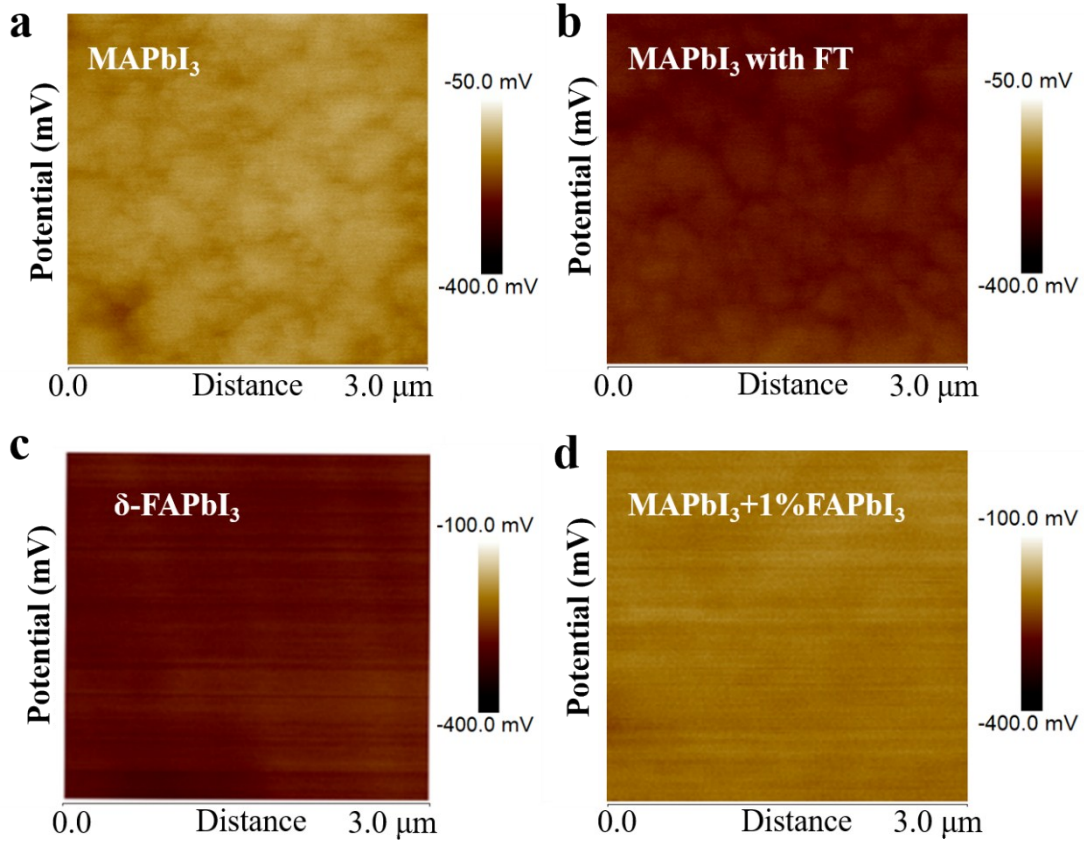


**Fig. S2** CPD mapping of (a) MAPbI<sub>3</sub>, (b) MAPbI<sub>3</sub> with FT, (c)  $\delta$ -FAPbI<sub>3</sub> and (d) MAPbI<sub>3</sub>+1%FAPbI<sub>3</sub> films at a scanning area of 3  $\mu$ m\*3  $\mu$ m from the surface.

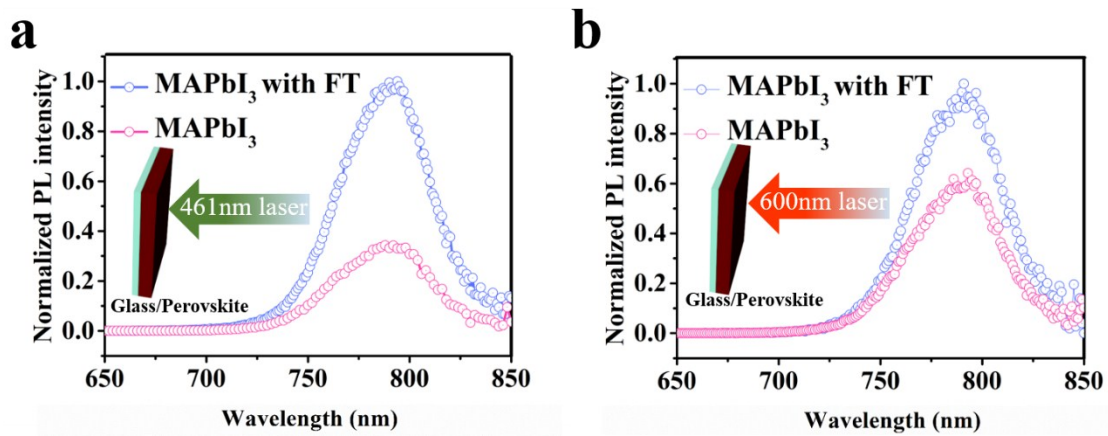


**Fig. S3** PL spectra of MAPbI<sub>3</sub> and MAPbI<sub>3</sub> with FT films excited by (a) 461 nm and (b) 600nm laser light, respectively. Note, the films were excited from above.

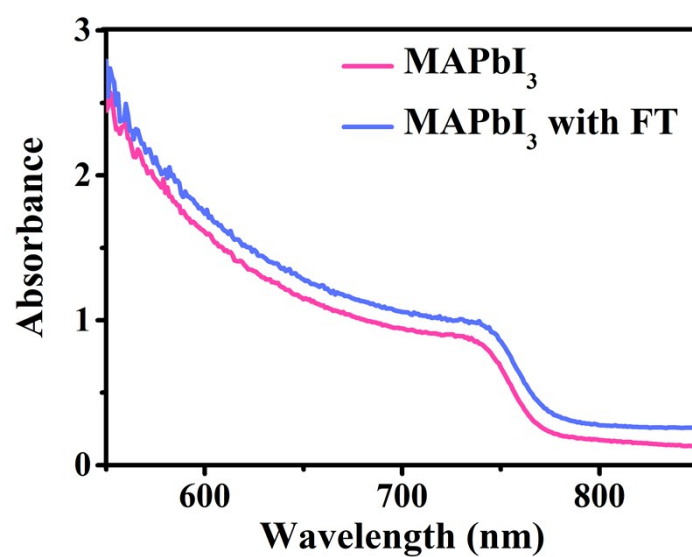


**Fig. S4** UV-visible absorption spectra of MAPbI<sub>3</sub> and MAPbI<sub>3</sub> with FT films.

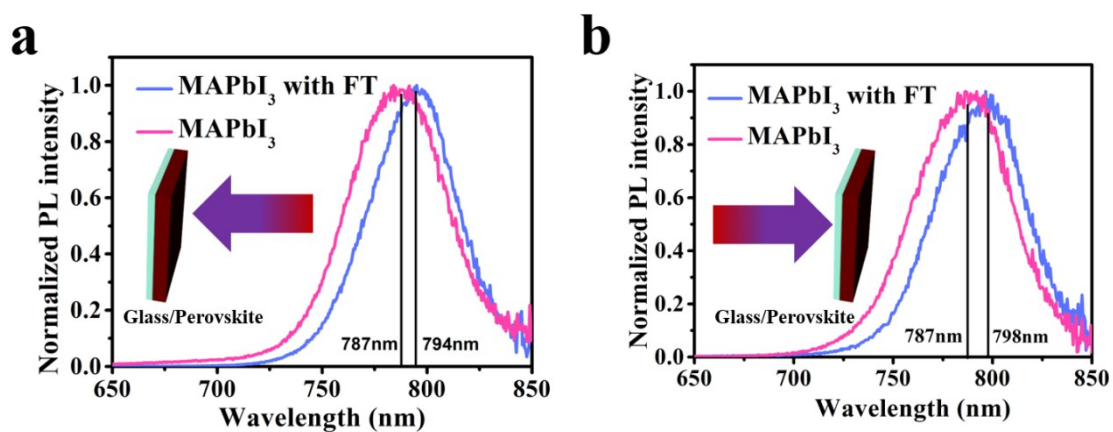


**Fig. S5** PL spectra of MAPbI<sub>3</sub> and MAPbI<sub>3</sub> with FT films excited from the (a) film side and (b) glass side, respectively.

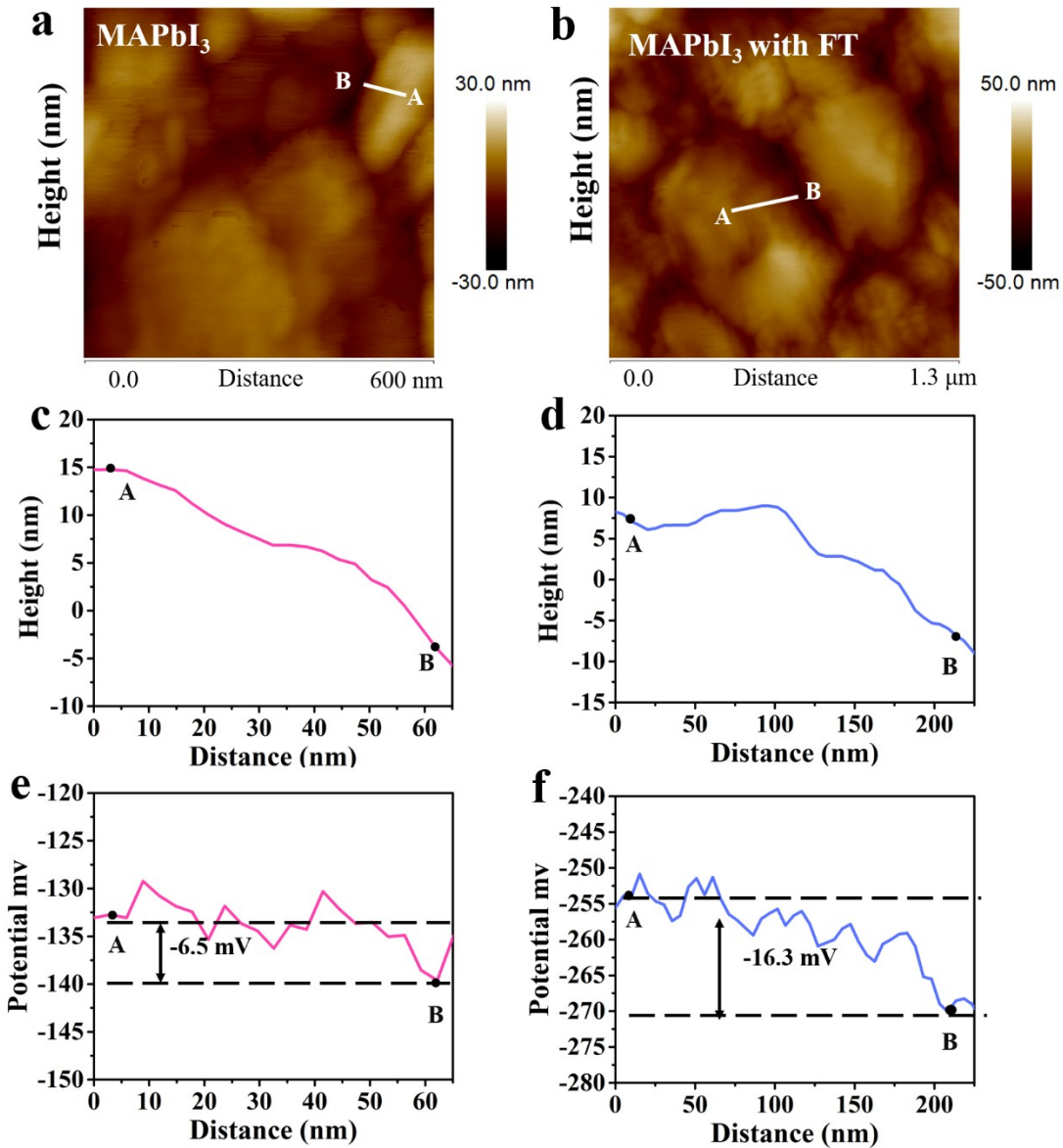


**Fig. S6** Topographic KPFM images of (a) MAPbI<sub>3</sub> and (b) MAPbI<sub>3</sub> with FT films. The height difference and CPD measured by the c-KPFM tip from the grain interior (position A) to GB (position B) as indicated on (c, e) MAPbI<sub>3</sub> and (d, f) MAPbI<sub>3</sub> with FT film, showed enhanced discrepancies of potential between the grain interior and GBs after FAI treatment, indicating possible composition/phase changes of the bulk perovskite upon FAI treatment.

For the MAPbI<sub>3</sub> film, the difference of contact potential between the grain interior and GB was -6.5 mV. Such a small variation was attributed to the intrinsic height difference of approximately 20 nm between the grain interior and GB (Fig. S6a,

6c and 6e). In contrast, an enlarged CPD discrepancy of up to -16.3 mV was observed for the MAPbI<sub>3</sub> with FT sample (Fig. S6b, 6d and 6f). The height difference between the grain interior and GBs of the selected position was also approximately 20 nm. Therefore, the considerable difference in CPD was chiefly attributed to the gradient composition/phase distribution and alteration, rather than the height difference. This result was in good agreement with the fact that both alloying FA/MA and the formation of  $\delta$ -FAPbI<sub>3</sub> results in a reduction (i.e., negative shift) of surface potential (see KPFM results in Fig. 1f and g). This negative shift of CPD was associated with the possible reaction between FAI and surplus PbI<sub>2</sub> at GBs and/or surface, and also ion diffusion and exchange of FA<sup>+</sup> with MA<sup>+</sup> cation in grain interiors, which alters the perovskite composition, thus inducing a gradient potential change from the grain interior to the GB.

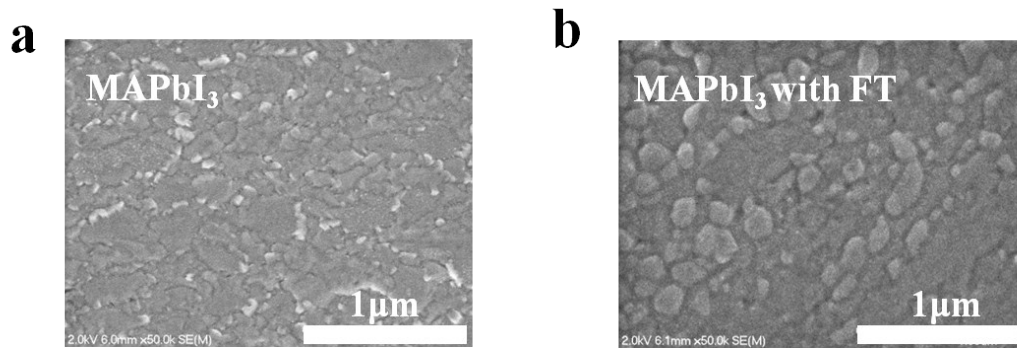


**Fig. S7** Top-view SEM images of (a) MAPbI<sub>3</sub> and (b) MAPbI<sub>3</sub> with FT films.

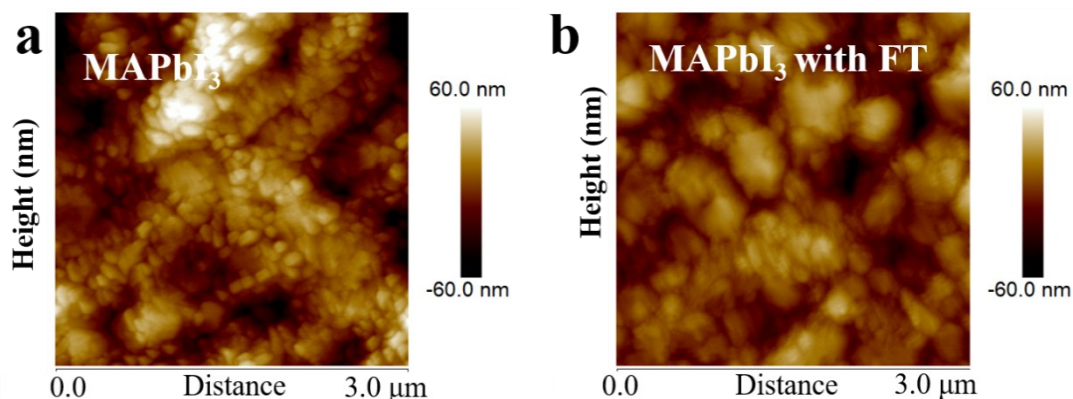


**Fig. S8** Topographic KPFM images showing the surface roughness of (a) MAPbI<sub>3</sub> and (b) MAPbI<sub>3</sub> with FT films.

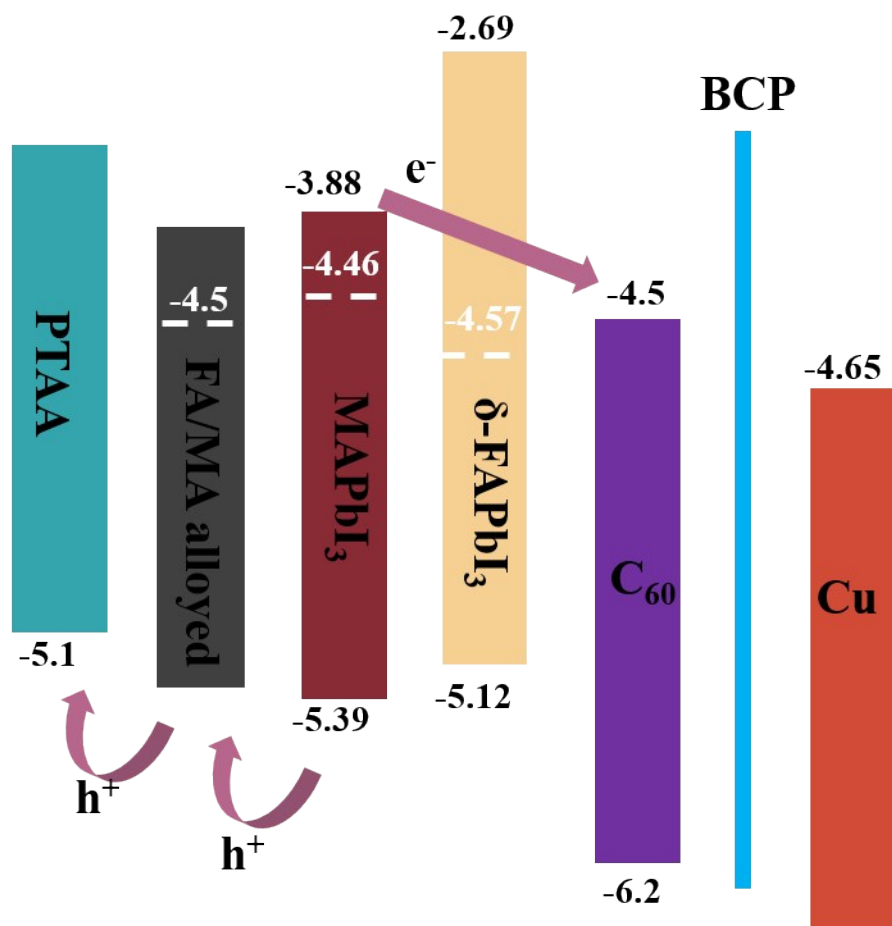


**Fig. S9** Energy level diagram of each functional layer within the completed PSCs. Note, the Fermi level was determined from the KPFM study, while the conduction band and valence band values are based on reported values.

The Fermi level of different perovskite compositions was determined according

to the equation,  $V_{CPD} = (\Phi_{tip} - \Phi_{sample})/e$ , where  $\Phi_{tip}$  and  $\Phi_{sample}$  represent the work function of the tip or sample, respectively, and  $e$  represents the elementary charge. Calculated Fermi levels were -4.46 eV, -4.50 eV and -4.57 eV for pristine MAPbI<sub>3</sub>, FA/MA alloyed perovskite and  $\delta$ -FAPbI<sub>3</sub>.

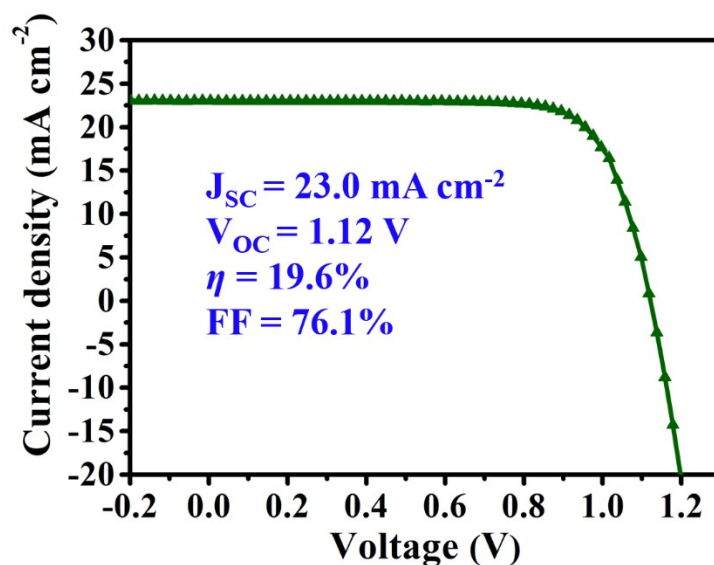


**Fig. S10**  $J$ - $V$  characteristics of a PSC based on the MAPbI<sub>3</sub>+1% FAPbI<sub>3</sub> thin film.

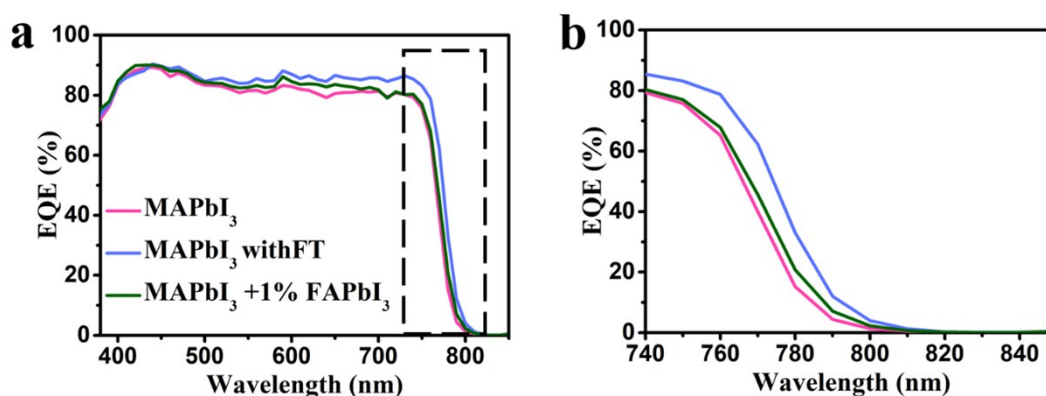


**Fig. S11** (a) IPCE spectra of PSCs based on MAPbI<sub>3</sub>, MAPbI<sub>3</sub> with FT and MAPbI<sub>3</sub>+1% FAPbI<sub>3</sub> films, and (b) an enlarged view showing the EQE onset.

**Table S1** The EQE onset and bandgap extracted and calculated from EQE spectra (Fig. 3f and S9).

PSCs	EQE onset /nm	Bandgap /eV
MAPbI <sub>3</sub>	789	1.57
MAPbI <sub>3</sub> with FT	799	1.55
MAPbI <sub>3</sub> +1% FAPbI <sub>3</sub>	795	1.56

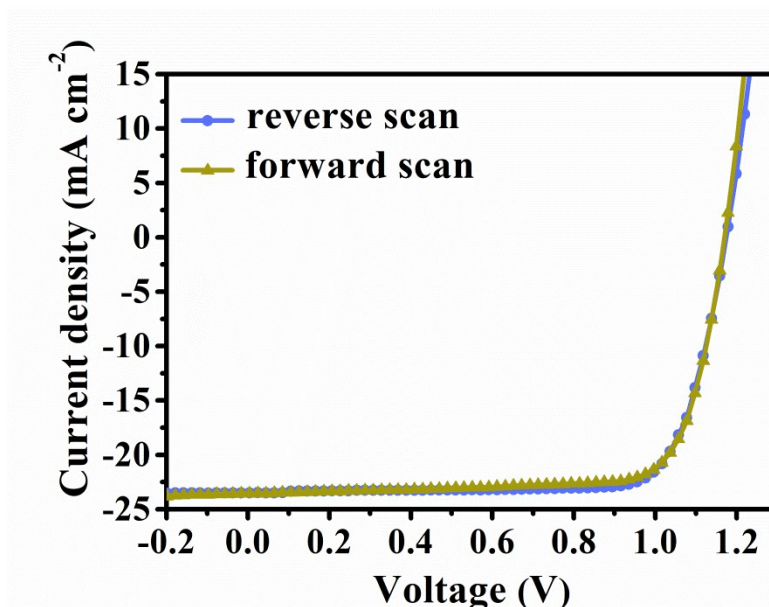


**Fig. S12**  $J$ - $V$  characteristics of the PSC based on the MAPbI<sub>3</sub> with FT film measured under different scanning directions at a scan rate of 0.1 V s<sup>-1</sup>.

**Table S2** Summarized photovoltaic parameters of PSCs based on the MAPbI<sub>3</sub> with FT film measured under AM 1.5 G illumination under different scan directions.

Scan direction	$J_{sc}$ /mA cm <sup>-2</sup>	$V_{oc}$ /V	$\eta$ /%	$FF$ /%
reverse scan	23.5	1.18	21.6	78.0
forward scan	23.6	1.18	21.3	77.0

**Table S3** A summary of the device performance for reported blade-coated PSCs based on different compositions and device structures.

<b>Perovskite composition</b>	<b>Device structure</b>	<b>PCE/%</b>	<b>Ref.</b>
MAPbI <sub>3</sub> treated with FAI	ITO/ PTAA/PVK/ /C60/BCP/Cu	21.9	This work
MAPbI <sub>3</sub>	ITO/PEDOT:PSS/PVK/PCBM/C60/BCP/Al	15.1	[1]
MAPbI <sub>3</sub>	ITO/PEDOT:PSS/PVK/PC <sub>61</sub> BM/C60-bis/Ag	12.21	[2]
MAPbI <sub>3</sub>	ITO/PEDOT:PSS/PVK/PCBM/C60/BCP/Al	12.8	[3]
MAIPbI <sub>3</sub> (Cl)	ITO/PEDOT:PSS/PVK/PCBM/C60/Ag	10.44	[4]
MAPbI <sub>3</sub>	FTO/c-TiO <sub>2</sub> /m-TiO <sub>2</sub> /PVK/Spiro/Au	4.5	[5]
FA <sub>0.4</sub> MA <sub>0.6</sub> PbI <sub>3</sub>	ITO/PTAA/PVK/PCBM/C <sub>60</sub> /BCP/Cu	18	[6]
MA <sub>0.6</sub> FA <sub>0.38</sub> Cs <sub>0.02</sub> PbI <sub>2.975</sub> Br <sub>0.025</sub>	ITO/PTAA/ PVK/PCBM /C60/BCP/Cu	19.3	[7]
MAIPbI <sub>3</sub> (Cl)	FTO/c-TiO <sub>2</sub> /PVK/Spiro/Ag	18.55	[8]
MAPbI <sub>3</sub>	FTO/TiO <sub>2</sub> /PVK/Spiro/Au	20	[9]
MAPbI <sub>3</sub>	ITO/PTAA/ PVK/PCBM /C60/BCP/Cu	20.3	[10]
MAPbI <sub>3</sub>	FTO/ TiO <sub>2</sub> / PVK /Spiro/Au	18.74	[10]
MAPbI <sub>3</sub>	ITO/ PVK/PCBM /C60/BCP/Cu	20.2	[11]

## References

- [1] Y. Deng, E. Peng, Y. Shao, Z. Xiao, Q. Dong, J. Huang, *Energy Environ. Sci.*, 2015, **8**, 1544-1550.
- [2] J. H. Kim, S. T. Williams, N. Cho, C. C. Chueh, A. K. Y. Jen, *Adv. Energy Mater.*, 2015, **5**, 1401229.
- [3] Y. Deng, Q. Wang, Y. Yuan, J. Huang, *Mater. Horiz.*, 2015, **2**, 578-583.
- [4] Z. Yang, C. C. Chueh, F. Zuo, J. H. Kim, P. W. Liang, A. K. Y. Jen, *Adv. Energy Mater.*, 2015, **5**, 1500328.
- [5] S. Razza, F. Di Giacomo, F. Matteocci, L. Cina, A. L. Palma, S. Casaluci, P. Cameron, A. D'epifanio, S. Licoccia, A. Reale, *J. Power Sources*, 2015, **277**, 286-291.
- [6] Y. Deng, Q. Dong, C. Bi, Y. Yuan, J. Huang, *Adv. Energy Mater.*, 2016, **6**, 1600372.
- [7] S. Tang, Y. Deng, X. Zheng, Y. Bai, Y. Fang, Q. Dong, H. Wei, J. Huang, *Adv. Energy Mater.*, 2017, **7**, 1700302.
- [8] M. Yang, Z. Li, M. O. Reese, O. G. Reid, D. H. Kim, S. Siol, T. R. Klein, Y. Yan, J. J. Berry, M. F. van Hest, *Nat. Energy.*, 2017, **2**, 17038.
- [9] M. He, B. Li, X. Cui, B. Jiang, Y. He, Y. Chen, D. O'Neil, P. Szymanski, M. A. Ei-Sayed, J. Huang, *Nat. Commun.*, 2017, **8**, 1-10.
- [10] Y. Deng, X. Zheng, Y. Bai, Q. Wang, J. Zhao, J. Huang, *Nat. Energy.*, 2018, **3**, 560-566.
- [11] W.-Q. Wu, Q. Wang, Y. Fang, Y. Shao, S. Tang, Y. Deng, H. Lu, Y. Liu, T. Li, Z. Yang, *Nat. Commun.*, 2018, **9**, 1-8.

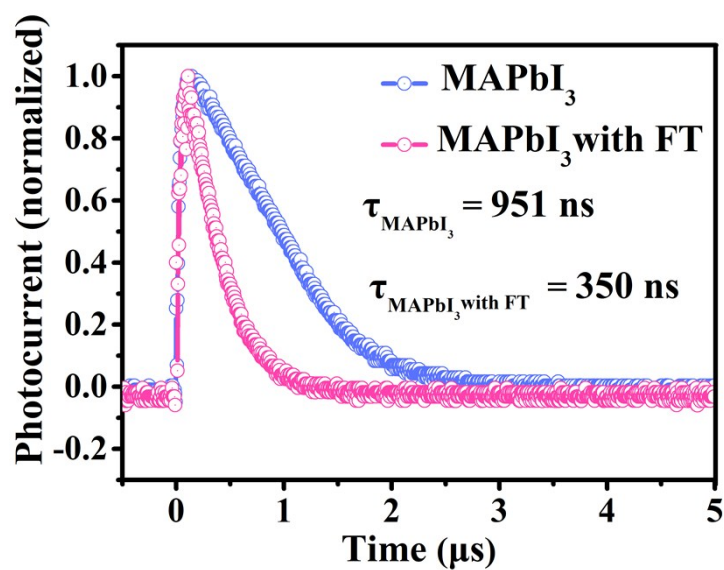


**Fig. S13.** TPC decay of the PSCs based on MAPbI<sub>3</sub> and MAPbI<sub>3</sub> with FT films.

**Table S4.** Summarized decay components for the samples based on the MAPbI<sub>3</sub> and MAPbI<sub>3</sub> with FT perovskite film sandwiched between PTAA and C<sub>60</sub> contacts. Values were extracted from the dynamic TA decay measurements in Fig. 4g.

Samples	$\tau_1/\text{ps}$	$A_1/\%$	$\tau_2/\text{ps}$	$A_2/\%$	$\tau_3/\text{ps}$	$A_3/\%$	Average /ps
MAPbI <sub>3</sub>	5840	10.9	17.1	26.5	883	62.7	3520.8
MAPbI <sub>3</sub> with FT	1140	14.6	999	32.3	189	53.1	900.9